Ciprofloxacin adsorption by biochar derived from co-pyrolysis of sewage sludge and bamboo waste

Jie Li[2] · Guangwei Yu[1] · Lanjia Pan[1] · Chunxing Li[3] · Futian You[1] · Yin Wang[1]

Abstract

Antibiotics residues in aqueous environment and sewage sludge accumulation have become serious environmental issues. The aim of this study is to investigate the potential of ciprofloxacin (CIP) removal by sludge-based biochar prepared from co-pyrolysis of sewage sludge and bamboo waste (BW). The stability and environmental risk of heavy metals (HMs) in the biochar were further investigated to evaluate potential risks for biochar utilization. Results showed that BW was an outstanding additive to prepare co-pyrolyzed biochar from sludge. A higher CIP removal rate (95%) of BW-sludge biochar (SBC) was obtained under initial CIP concentration of 10 mg/L, and its maximum adsorption capacity was 62.48 mg/g which was calculated from the Langmuir model. The pseudo-second-order and Freundlich model also well fit the CIP adsorption process, indicating a chemical and multilayer adsorption of CIP on a heterogeneous surface of biochar. Adsorption mechanism analysis indicated that the diverse functional groups and Fe species in biochar probably were the dominant factors in the adsorption of CIP. The π-π interaction, H–bond, ion exchange, and Fe-complexation might be the main interactions between the functional species and CIP molecules. Besides, HMs, especially the Cr, Cd, and As, were well immobilized in SBC compared with pure sludge biochar. This work suggested that sludge-based biochar, especially the co-pyrolyzed SBC, could be a potential adsorbent for CIP removal from aqueous solutions.

Keywords Biochar · Biomass · Pyrolysis · Ciprofloxacin · Adsorption · Heavy metals

Introduction

With the fast development of social economy and rapid urbanization, large amounts of sewage sludge (SL) are generated in municipal sewage plants. In 2016, around 13 million tons (dry weight) of SL were produced in China, and its amount is

✉ Guangwei Yu
  gwyu@iue.ac.cn

[1] Key Laboratory of Urban Pollutant Conversion, Institute of Urban Environment, Chinese Academy of Sciences, Xiamen 361021, China

[2] Department of Chemical and Biomolecular Engineering, National University of Singapore, Singapore 117585, Singapore

[3] Department of Environmental Engineering, Technical University of Denmark, DK-2800 Kgs. Lyngby, Denmark

predicted to continuously increase with an annual rate of approximately 10% over a 10-year period (Jin et al. 2017). Therefore, SL remains a great concern due to its abundance of contamination, including heavy metals (HMs), microorganisms, and hazardous organic substances (Fytili and Zabaniotou 2008). How to safely treat SL and utilize its byproduct is becoming an impending problem. Pyrolysis is a thermal degradation process within an inert atmosphere, which has been proved to be an effective strategy for SL treatment with generation of sewage sludge biochar (SLC), biogas, and oil (Frišták et al. 2018). The organic pollutants, e.g., pathogens and antibiotics, could be degraded thoroughly, and the leaching concentrations of HMs can be also reduced (Dou et al. 2017; Wang et al. 2016).

In addition, antibiotics residues in aqueous environment have caused many serious environmental problems in recent years. Ciprofloxacin (CIP), a second-generation quinolone, has been frequently detected in aquatic environment, including ground, surface, and even drinking water, due to its chemical stability and ability for bacteria inhabitation (Mao et al. 2016). It is reported that CIP concentration in waste water

reaches 31 mg/L, and this value is even higher in wastewater stream of drug plants (Zhang et al. 2017). CIP does harm to human health due to emerging and acute genotoxicity (Espinosa et al. 2015; Li et al. 2014). Researchers have explored many methods, including adsorption, oxidation, and photolytic/photocatalytic and biological treatment, to eliminate CIP from contaminated water (Liao et al. 2016; Tu et al. 2014; Zhang et al. 2017). Among these approaches, adsorption is one of the most promising technologies for its high efficiency and simple operation (Zhu et al. 2015).

SLC could be a potential low-cost adsorbent for CIP removal due to its specific physicochemical properties owing to its rich functional groups, developed micropores and mesopores, and some special metal elements (Li et al. 2015a; Ren et al. 2018). Our previous study has found that a catalyst prepared from the SLC facilitated a CIP adsorption ability (Li et al. 2019). Another previous research in our group has proved that CIP molecules could be easily attracted by a biochar surface with various functional groups (Li et al. 2018). Besides, it has been reported that 66.70% of CIP was removed by a biochar prepared from sludge as humic acid increased the degradation ability of •OH, while its removal performance could be further improved (Luo et al. 2019). One feasible approach to improve adsorption ability of biochar is optimizing its physicochemical properties, e.g., pore structure, functional groups, and elements components by co-pyrolysis with other additives (Fan et al. 2016; Thines et al. 2017; Zhao et al. 2018). Authors stated that co-pyrolysis of SL and other biomasses can adjust microstructure and compositions of biochar, especially the contents of C, H, N, and organic matter (Huang et al. 2017; Jin et al. 2017), which might elevate the adsorption ability of CIP. Moreover, previous studies reported that pyrolysis or hydrothermal treatment of sludge with other additives could minimize the environmental risks from metals (Jin et al. 2017; Xie et al. 2019). As far as we know, previous research has investigated little about CIP adsorption by sewage sludge biochar, much less by the biochar derived from co-pyrolysis of SL and BW.

For this study, the bamboo waste (BW) with high organic matter content was chosen as biomass addictive to co-pyrolyze with SL. Two significant benefits may be obtained from the co-pyrolysis of SL with BW. First, much more biogas and biooil can be produced after the BW addition due to its high content of organic components. These biofuels can be used for energy supply in the co-pyrolysis process to save extra energy and avoid carbon emission. Second, the characteristics of biochar from the co-pyrolysis will be improved, e.g., enrichment of the surface functional groups and decrease of the HM contents in biochar, which can extent the application of sludge-based biochar and make a contribution on solving the terminal utilization problem of sludge treatment byproduct. In this work, biochar samples from single SL and mixture of SL and BW were prepared via pyrolysis to obtain a

low-cost and safe adsorbent with high CIP adsorption ability, and they were characterized on the adsorption performance of CIP from aqueous solution. Furthermore, the kinetics and isotherms of CIP adsorption were investigated and the possible adsorption mechanism was according to the characterization analysis of biochar. In addition, the speciation, leaching behavior, and potential ecological risk from HMs were analyzed to evaluate its potential of utilization.

Materials and methods

Raw materials and biochar preparation

CIP with analytical standard was obtained in Aladdin Industrial Corporation which is located in Shanghai, China. Other analytical-grade chemicals were purchased from Sinopharm Chemical Reagent Co., Ltd., China. SL was taken from a sewage plant located in in Xiamen City, Fujian province. BW was collected from the same city and ground to less than 150 μm after being dried in an oven at 105 °C for 24 h. As can be seen in Table 1, the proximate and ultimate analysis of raw materials, i.e., SL and BW, were analyzed before experiments.

SL and mixture of SL and BW (mass ratio of 4: 1) were introduced into a pyrolysis reactor to prepare biochar. Pyrolysis was conducted in a vertical tubular furnace at 700 °C with a ramp rate of 10 °C/min within nitrogen atmosphere for 30 min. These operational parameters were chosen from our previous work which found that the ratio and processing conditions have a positive effect on the immobilization of heavy metals in sludge and porous structure of biochar (Wang et al. 2019a, b, c). After pyrolysis finished, SL-based biochar (SLC) and BW-sludge-based biochar (SBC) were collected to keep in a desiccator for subsequent experiments.

Adsorption experiments

According to our previous work (Li et al. 2018), the two types of biochar were weighed as 0.25 g and added into 100 mL of CIP solutions, and then batch adsorption experiments were conducted under conditions of pH of 6.0 and temperature of 30 °C, respectively. The CIP solution was put into sealed flasks which were placed in a shading shaker with a speed of 200 rpm for 24 h. For the adsorption kinetic study, the 10 mg/L CIP solution was used, and samples were withdrawn at interval times (0 h, 1 h, 2 h, 5 h, 8 h, 12 h, 24 h) during 24 h with a small volume of 0.5 mL each time. For the equilibrium adsorption isotherm, five different initial concentrations (5, 10, 20, 50, 100, and 200 mg/L) were selected with the contact time of 24 h. The batch experiments were conducted in triplicate. The CIP concentration of the solution sample taken from the flasks was detected by the high-performance liquid

Table 1 Proximate and ultimate analysis of SL and BW

Items	Moisture (wt.%)	Proximate analysis (wt.%, d)			Ultimate analysis (wt.%, d)				
		Ash	Volatiles	Fix carbon	C	H	N	S	$^{a}O_{diff.}$
SL	80.17	46.55	48.07	5.38	24.69	3.71	3.71	0.85	20.49
BW	6.43	3.21	77.91	18.88	36.32	4.90	0.04	0.60	54.93

^{a} $O_{diff.}$ = 100-C-H-N-S-Ash

chromatography (HPLC, Hitachi L-2000, Japan) after filtered through a 0.45-μm membrane. The details of the detected conditions and method have been reported in our previous study (Pan et al. 2018).

The amount of CIP adsorption and its removal percentage were computed via Eqs. (1)–(3), respectively (Hairuddin et al. 2019).

$$q_t = \frac{C_0 - C_t}{M} \cdot V \tag{1}$$

$$q_e = \frac{C_0 - C_e}{M} \cdot V \tag{2}$$

$$RP = \frac{C_0 - C_e}{C_0} \cdot 100 \tag{3}$$

where the q_t (mg/g) represents the amount of CIP adsorbed by biochar at contact time of t (h); q_e (mg/g) means the amount of CIP adsorption at equilibrium; C_0 (mg/L) represents the initial concentration of CIP; C_t is the CIP concentration at contact time of t; C_e (mg/L) is the CIP concentration after reaching adsorption equilibrium; V (L) means the volume of CIP solution; M (g) is biochar mass added in the solution; and RP (%) is the removal percentage of CIP from the solution.

Adsorption kinetic analysis

In order to understand the adsorption process, three adsorption kinetic models were analyzed. Besides, the normalized standard deviation (Δq) was employed to quantitatively compare the applicability of the model in fitting the data. A lower value of Δq (%) indicates a better fit of the kinetic models (Nasuha et al. 2010).

Pseudo-first-order model:

$$q_t = q_e\left(1 - e^{-k_1 t}\right) \tag{4}$$

Pseudo-second-order model:

$$q_t = \frac{q_e^2 t k_2}{1 + k_2 q_e t} \tag{5}$$

Intra-particle diffusion model:

$$q_t = k_{id} t^{1/2} + C \tag{6}$$

Normalized standard deviation:

$$\Delta q = 100 \times \sqrt{\frac{\sum\left[\left(q_{t,exp} - q_{t,cal}\right)/q_{t,exp}\right]^2}{n-1}} \tag{7}$$

where q_t (mg/g) and q_e (mg/g) are the amounts of CIP adsorbed by biochar at contact time and equilibrium, respectively; k_1 (h^{-1}), k_2 (g/(mg h)), and k_{id} (mg/g h$^{-1/2}$) are the rate constants of pseudo-first-order, second-order, and intra-particle model, respectively; C is the boundary layer thickness; $q_{t,exp}$ represents the experimental data; $q_{t,cal}$ (mg/g) is the values calculated from kinetic models at contact time of t; n is the number of total data samples.

Adsorption isotherm analysis

To evaluate the CIP-biochar interaction at adsorption equilibrium state, typical adsorption isotherm models, including Langmuir, Freundlich, and Redlich–Peterson models with nonlinear forms, were investigated (Karri et al. 2017; Tran et al. 2017b), as seen in Eqs. (8–11):

Langmuir isotherm equation:

$$q_e = \frac{q_{max} K_L C_e}{1 + K_L C_e} \tag{8}$$

$$R_L = \frac{1}{1 + K_L C_0} \tag{9}$$

Freundlich isotherm equation:

$$q_t = K_F C_e^n \tag{10}$$

Redlich–Peterson equation:

$$q_e = \frac{K_{RP} C_e}{1 + a_{RP} C_e^g} \tag{11}$$

where q_{max} (mg/g) indicates the theoretical maximum of adsorption amount; R_L is a parameter of dimensionless; C_0 (mg/L) and C_e (mg/L) are the initial and equilibrium concentrations of CIP; K_L and K_F are the constants in Langmuir and Freundlich models; n represents an indicator of magnitude of the adsorption driving force or surface heterogeneity; and K_{RP} (L/g) and A_{RP} (mg/L)$^{-g}$ are the constants of Redlich–Peterson, and g

(dimensionless) is its exponent with a value between 0 and 1.

Characterization of biochar

The proximate analyses including moistures of sludge and bamboo waste were conducted according to Chinese government standard (GB/T 2873-2012: Proximate analysis of solid biofuels). Ultimate analysis of raw and biochar samples was conducted by Vario MAX (Elementar Analysensysteme GmbH, Germany). The values of H/C, O/C, and (O + N)/C ratios were further calculated from the ultimate. The pore structure of biochar including pore-size and specific surface areas (calculated by Brunauer-Emmett-Teller (BET) method) was analyzed based on the N_2 adsorption/desorption isotherms in a volumetric system (Micromeritics ASAP 2020 M+C, USA). Scanning electron microscopy (SEM, Hitachi S-4800, Japan) was carried out for the morphology of SLC and SBC, and X-ray photoelectron spectroscopy (XPS, ThermoFisher Scientific XLESCALAB250Xi, UK) was employed to analyze its surface chemical states.

Results and discussion

Biochar characterization

Ultimate analysis of biochar

From the ultimate analysis of biochar (Table 2), it was found that adding bamboo into sludge could elevate C contents of biochar. The SBC had a higher total carbon content of 22.70% compared with SLC (15.55%), due to the high contents of C in BW. Furthermore, aromaticity, hydrophilia, and polarity of biochar can be analyzed based on the values of O/C, H/C, and (O+N)/C ratios, respectively (Agrafioti et al. 2014). As shown in Table 2, the H/C values of the two biochar were extremely low, which implied that the biochar was almost completely carbonized with high aromaticity produced (Han et al. 2016). Furthermore, both of the two biochar samples possessed a low H/C ratio and high (O+N)/C, suggesting their high carbonization and polarity. Compared with SLC, O/C ratios of SBC were much lower, which implied that the hydrophilicity of SBC may be lowered to some extent after co-pyrolysis with BW.

Table 2 Ultimate analysis of biochar samples (wt.%, d)

Items	C	H	N	S	O[a]	H/C	O/C	(O+N)/C
SLC	15.55	0.86	1.18	0.51	35.35	0.06	2.27	35.43
SBC	22.70	0.82	1.07	0.62	36.91	0.04	1.63	36.96

[a] O_{diff} = 100-C-H-N-S-Ash

Porous structure and micrographs analysis of biochar

According to the results of porous structure analysis (Fig. 1), both of the two types of biochar had a type H3 hysteresis loop, which indicated that biochar obtained from co-pyrolysis had a slit-like mesoporous structure due to the generation of plate-like particles in the pyrolysis (Thommes et al. 2015; You et al. 2017). The pore structure analysis results of biochar are shown in Table 3. The BET surface area (47.48 m^2/g) of SBC was much higher than that of SLC (25.68 m^2/g). This result implied that addition of BW could enhance the BET surface of sludge-based biochar significantly. However, the average pore size was decreased after the adding of BW in the SL pyrolysis. The reason may be that main C–C bonds of BW were cracked, and then, short-chain products reacted with the functional groups of SL and fill in the pores of SBC during co-pyrolysis (Miskolczi and Nagy 2012).

Figure 2 presents the SEM micrographs of SLC and SBC. SLC was made up of many blocks with various shapes, including rod-like, atactic and stratified structures. In addition, there were some slit pores distributed irregularity due to the blocks' stacking in SLC, while many spherical particles appeared and attached on the blocky structure in SBC after the co-pyrolysis of SL with BW. Besides, the blocks became smaller and the slit pores were narrower compared with SLC. This may be the reason why SBC obtained a higher specific surface area than that of SLC. This result of the SEM micrograph analysis was consistent with that of the porous structure analysis.

Surface species analysis of biochar

The characteristics of C 1s and Fe 2p for SLC and SBC were determined by XPS. As shown in Fig. 3 and Table 4, the peaks of both the SLC and SBC can be separated into four identical peaks that appeared at 284.34 (or 284.35), 284.75 (or 284.73), 285.2, and 286.35 eV, respectively. The peaks at 284.34 (or 284.35) and 284.75 (or 284.73) indicated the existence of C–C, aromatic C–H, and aliphatic hydrocarbons (Shen et al. 2017). The peak position located at 285.20 eV corresponds to C=O or C–O–C groups, and the functional groups of C–OH or C≡N was also proven to exist according to the peak at 286.35 eV (Dementjev et al. 2000; Jiang et al. 2013; Shen et al. 2017). However, all the peak contents in SBC were higher than those in SLC except the peak at 284.35 eV. Fe species in the biochar was also detected due to its high content in SL (Li et al. 2017a). Literature reported that the biochar modified by Fe possessed high adsorption ability owing to strong interaction of Fe species and adsorbate in solution from the electrostatic reaction and metal precipitation (He et al. 2012). Our previous study also found that biochar-based catalyst with rich Fe species equipped both adsorption and catalytic degradation ability of CIP (Li et al. 2017a). Hence, the
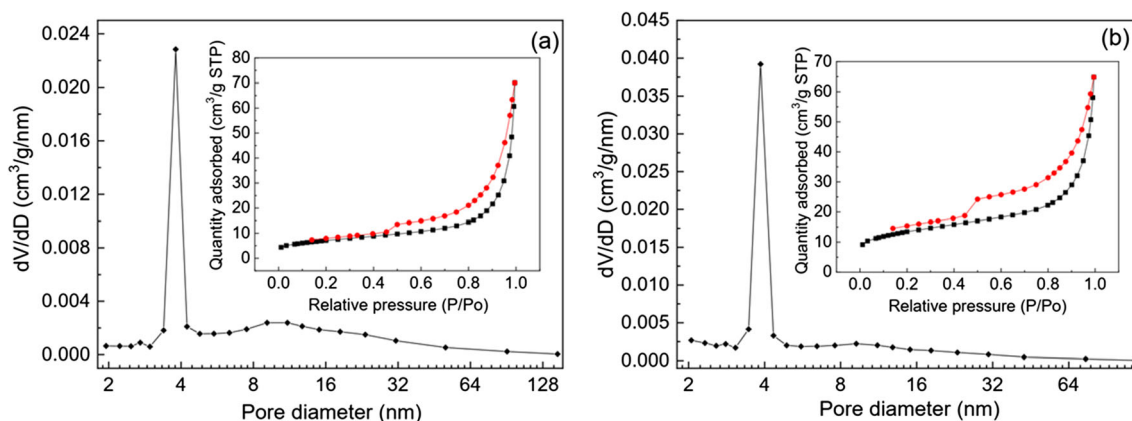
Fig. 1 Nitrogen adsorption-desorption isotherms and pore distribution of SLC (**a**) and SBC (**b**)

characteristics of Fe species in biochar were analyzed via XPS for further understanding of the CIP adsorption mechanism on sludge-based biochar. As shown in Fig. 3, two peaks of Fe species (Fe $2p_{3/2}$ and Fe $2p_{1/2}$) were detected in the two types of biochar. Both of the Fe $2p_{3/2}$ peaks were stronger and narrower than the peaks of Fe $2p_{1/2}$. It was reported that the stronger Fe $2p_{3/2}$ peaks in biochar were generated from spin–orbit (j–j) coupling (Grosvenor et al. 2004). Moreover, the shapes of the two peaks were quite close to those of Fe_3O_4, indicating that both Fe^{2+} and Fe^{3+} existed in sludge-based biochar (Yamashita and Hayes 2008). In details, the peaks were deconvoluted into two peaks of Fe^{2+} and Fe^{3+} according to their peak positions reported in the literature (Grosvenor et al. 2004). Comparing the two biochar, they possessed the same split peak, while the relative contents of Fe $2p_{3/2}$ peak for Fe^{3+} at 714.60 eV and the satellite for Fe^{2+} at 711.20 eV appeared in SBC were much higher than that in SLC.

Adsorption of CIP by biochar

Adsorption kinetics studies

The CIP solution samples were taken at different adsorption times to analyze the change of CIP concentration during the biochar adsorption process. As can be seen in Fig. 4a, the C_t declined with a fast speed at the beginning of 2 h, and then the reduction rate of CIP concentration became slow. The plateaued state reached under condition of adsorption time of more than 12 h. The rapid adsorption rate at the beginning was probably due to the high difference of CIP concentration between the solution and surface of the biochar containing large amounts of free active sites from the function species (Chang et al. 2014;

Cheung et al. 2007; Yamashita and Hayes 2008). In addition, the value of removal percentage (RP), obtained by SBC adsorption, was 95% which increased by 8% compared with RP of SLC. Furthermore, fitting results of three adsorption kinetic models based on the data of CIP concentration at different times are demonstrated in Fig. 4b, c and Table 5. The value of R^2 from the pseudo-second-order model fitting was 0.99 which was much higher than that of the pseudo-first-order. This showed that CIP adsorption onto biochar was well fitted by using pseudo-second-order kinetic model, revealing that CIP adsorption by sludge-based biochar was a chemical adsorption process, and the number of free active sites on the surface of biochar was significantly related to its adsorption capacity (Li et al. 2015b). The rate constants of the second-order model (k_2) of SLC and SBC were 0.67 and 0.63, implying a fast CIP adsorption rate onto the biochar (Ahmad et al. 2012).

Literature has reported that absorbing rate is mainly controlled by intra-particle or boundary layer diffusion, or both of them (Sun et al. 2016). In this work, the adsorption process of biochar could be separated into three linear portions within the whole adsorption time based on the intra-particle diffusion model analysis (Fig. 4d). The first sharper portions indicated fast diffusion of CIP molecules to outer surface of the biochar. The second portions with smaller slopes described gradual penetration of CIP molecules into micropores and mesopores of the biochar due to greater resistance that occurred. In this case, the slope of the second portion in the SBC adsorption process was much greater, suggesting a lower resistance or stronger adsorption ability for CIP, compared with SLC. The third portions suggested that the state of CIP adsorption approached to equilibrium. Another notable result was that the first linear portion did not pass through the origin

Items	BET surface area (m²/g)	Pore volume (cm³/g)	Average pore size (nm)
SLC	26 ± 2	0.11 ± 0.01	14 ± 4
SBC	47 ± 5	0.09 ± 0.01	9 ± 2

Table 3 Pore structure analysis of biochar

Fig. 2 SEM micrographs of SLC (**a**) and SBC (**b**)
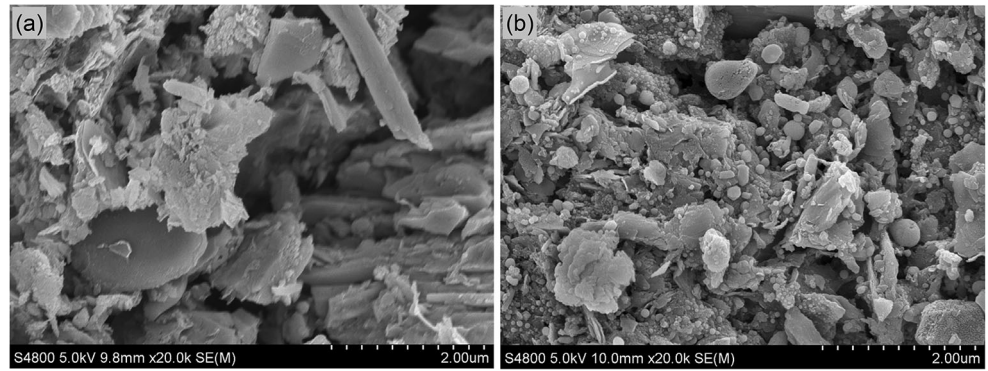
point, which indicated that the adsorption process was mainly limited by both boundary layer and intra-particle diffusion (rate-controlling steps). This meant the adsorption process in our experiments was not only related to the mass transfer of CIP but also to the diffusion in the internal pore and on the surface of biochar. For the behaviors and kinetics of mass transfer of CIP adsorption, it will be further investigated using the mass transfer kinetics in our future work, which will be of benefit to better understand the adsorption mechanism (Fulazzaky 2011; Fulazzaky et al. 2013, 2017).

Adsorption isotherm studies

Figure 5a presents the CIP adsorption capability of biochar under the condition of different initial concentrations. The q_e elevated gradually with elevation of initial CIP concentrations due to increasing of driving force from the concentration gradient. This driving force was able to conquer the resistance and obstruction from the CIP diffusion between the solution and solid phases of biochar (Srivastava et al. 2006). For the RP of CIP by biochar, there were different trends for CIP adsorption on the biochar with a rising of the initial CIP
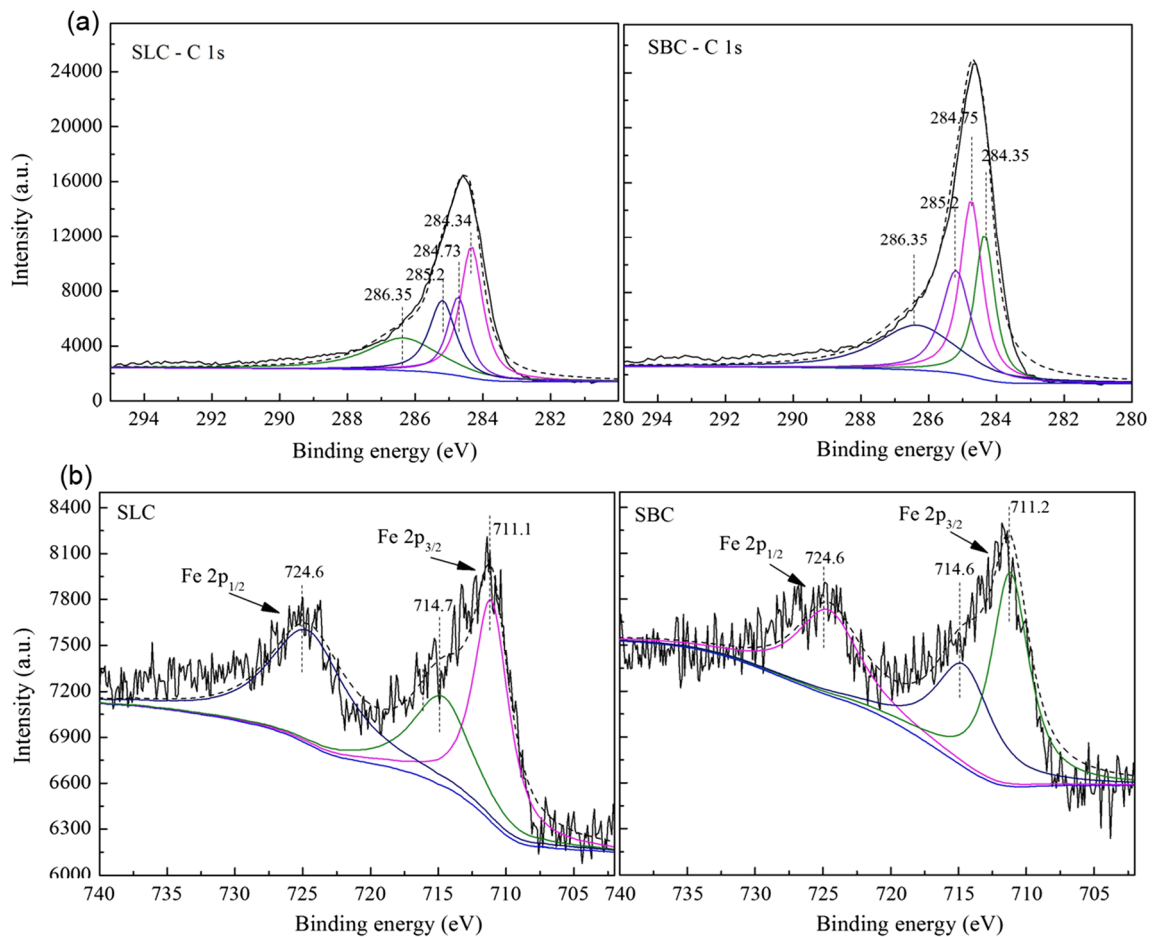

Fig. 3 C 1s (**a**) and Fe 2p (**b**) XPS spectra of SLC and SBC

Table 4 The relative content of functional groups in biochar detected by XPS

Element	Position (eV)	Contents (%)		Functional groups and Fe valence
		SLC	SBC	
C 1s	284.34 (284.35)	33.50	21.64	C–C, C–H
	284.75 (284.73)	18.79	29.30	C–C, C–H
	285.20	21.61	22.23	C=O, C–O–C, C–N, C=N
	286.35	26.10	26.83	C–OH, C≡N
Fe 2p$_{1/2}$	724.6	40.27	27.64	Fe^{3+}
Fe 2p$_{3/2}$	711.10 (711.20)	35.76	41.70	Fe^{3+}
Satellite	714.70 (714.60)	23.97	30.67	Fe^{2+}

concentration. The RP of SLC kept at high values (90%) at the range of initial CIP concentration from 5 to 10 mg/L due to their adequate active sites. However, the RP of SBC first increased and then decreased with the initial CIP concentration increasing, and the maximum RP was 95% under the condition of initial CIP concentration of 10 mg/L. With the initial CIP concentration elevating continuously from 10 to 200 mg/L, the RP of the two types of biochar decreased significantly due to finite functional groups and active sites on the surface of biochar.

In addition, three adsorption isotherm models were employed to explore the adsorption process of biochar under different initial CIP concentrations (Fig. 5). The model fitting results including regression coefficients (R^2) and other constants of adsorption isotherm models are shown in Table 6.

The R^2 of fitting with Langmuir isotherm was 0.92 and 0.91 for the CIP onto SLC and SBC, and the maximum adsorption capacity could be obtained after fitting. The maximum adsorption capacities of SLC and SBC for CIP adsorption were 46.20 and 62.48 mg/g which were higher than those of many other biochar prepared from different feedstocks (Table 7). Besides, the Freundlich model exhibited a better fit ($R^2 = 0.99$) for CIP adsorption by the two types of biochar compared with Langmuir. It can be inferred that the surface of biochar was heterogeneous, on which the CIP molecules were adsorbed with multilayer (Foo and Hameed 2010). Moreover, K_F is an indication of the adsorbent capacity and n is an index of the adsorption intensity and surface heterogeneity. $1 > n > 0$ in this work indicated that the adsorption intensity and surface heterogeneity were moderate (Haghseresht and Lu 1998).
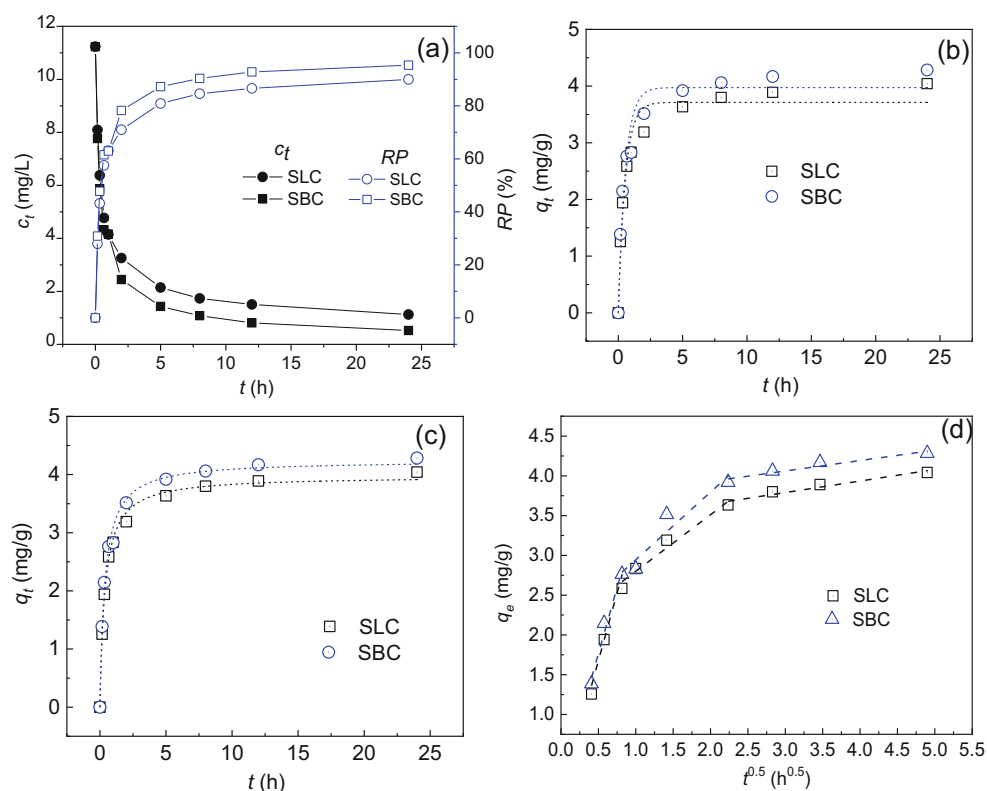

Fig. 4 Kinetic studies for the adsorption of CIP by biochar: Time effect (**a**), pseudo-first (**b**), pseudo-second (**c**), intra-particle diffusion (**d**)

Table 5 Kinetic parameters for the adsorption of CIP by biochar

Kinetic models	Parameters	SLC	SBC
	$q_{e,\exp}$ (mg/g)	4.04	4.28
Pseudo-first-order parameters	k_1	1.85	1.82
	$q_{e,\text{cal}}$ (mg/g)	3.71	3.97
	R^2	0.91	0.89
	$\triangle q$ (%)	11.20	13.10
Pseudo-second-order parameters	$q_{e,\text{cal}}$ (mg/g)	3.97	4.24
	k_2	0.67	0.63
	R^2	0.99	0.99
	$\triangle q$ (%)	2.91	4.72
Intra-particle diffusion parameters	$k_{\text{id}1}$	3.22	3.32
	C_1	0.00	0.10
	R_1^2	0.97	0.95
	$k_{\text{id}2}$	0.71	0.85
	C_2	2.09	2.09
	R_2^2	0.95	0.89
	$k_{\text{id}3}$	0.14	0.13
	C_3	3.36	3.67
	R_3^2	0.92	0.90

Table 6 Isotherm parameters for CIP adsorption by different biochar

Isotherms	Parameters	SLC	SBC
Langmuir	$q_{\max}$ (mg/g)	46.20	62.48
	K_L	0.015	0.009
	R^2	0.92	0.91
	R_L	0.62	0.71
Freundlich	K_F	2.55	2.68
	n	0.51	0.52
	R^2	0.98	0.96
	K_{RP}	1.17×10^5	2.14×10^5
Redlich–Peterson	A_{RP}	4.6×10^4	8.0×10^4
	g	0.49	0.48
	R^2	0.97	0.95

equation becomes the Langmuir equation with $g = 1$, and it will transform into the Freundlich isotherm when K_{RP} and $a_{KP} \gg 1$ and $g = 1$. In this work, the fitting result showed that K_{RP} and $a_{KP} \gg 1$, while g was not equal to 1. This may further indicate that the CIP adsorption process approached the Freundlich isotherm (Tran et al. 2017b).

Comparing the two types of biochar, the higher K_F of SBC indicated a higher CIP capacity, which agreed with the result of the Langmuir model. Moreover, the Redlich–Peterson model was further investigated, because it includes the features of both Langmuir and Freundlich. The Redlich–Peterson

Adsorption mechanism

From the above analysis of the characteristics of the two biochar, although the was a significant difference in O/C ratios (a hydrophilicity index), micrographs, and pore structures (much

Fig. 5 Adsorption isotherm for the adsorption of CIP by biochar: Initial CIP concentration effect (**a**), Langmuir model fitting (**b**), Freundlich model fitting (**c**), and Redlich–Peterson model fitting (**d**)
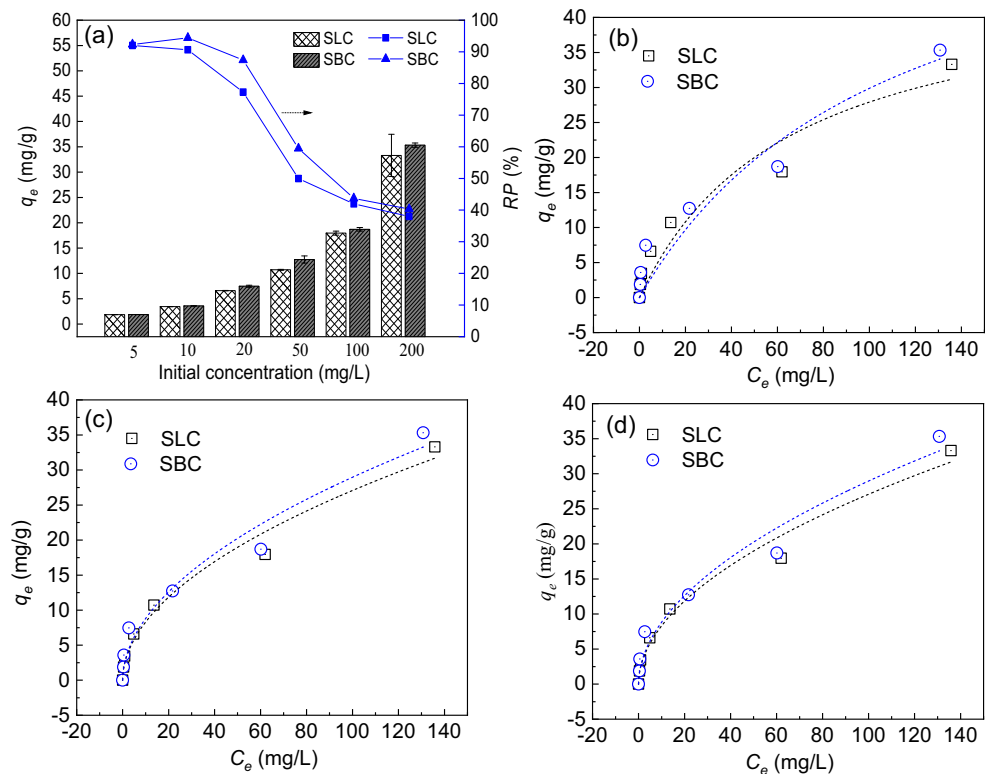
Table 7 Comparison of the maximum adsorption capacity and model fitting performance of biochar in this work and literatures

Adsorbents	Maximum adsorption capacity (mg/g)	R^2 of Langmuir	R^2 of Freundlich	Reference
Used tea-leaf biochar	238.10	0.99	0.99	Li et al. 2018
Rice straw biochar	76.69	0.96	0.98	Zeng et al. 2018
Herbal residue biochar	43.67	0.99	0.98	Shang et al. 2016
Chitosan/biochar hydrogel beads	78.79	0.99	0.94	Afzal et al. 2018
Potato waste biochar	8.48	0.94	0.92	Li et al. 2017b
KOH-modified potato waste biochar	23.36	0.90	0.89	Li et al. 2017b
Water hyacinth biochar	2.72	0.99	0.99	Ngeno et al. 2016
Sludge biochar	46.20	0.92	0.98	This work
Sludge-bamboo biochar	62.48	0.91	0.96	This work

higher BET surface area and smaller pore size for SBC) between the two biochar, the CIP adsorption ability of SBC exhibited slight elevation (8%). The results indicated that the hydrophilicity and pore structure of sludge-based biochar probably were not the dominated factors for the CIP adsorption in the range of this study. This result was consistent with what concluded in our previous study on the investigation of CIP adsorption on waste tea–based biochar (UTC). It was found that the UTC with a low BET surface area (8.06 m^2/g) still facilitated a good CIP adsorption ability (Li et al. 2018).

Another notable result was that both of the two biochar obtained an outstanding CIP adsorption. According to the XPS analysis, C–C and C–H were detected, indicating that there were alkanes or aromatic rings existing in the biochar. Therefore, the π-π donor-acceptor interactions between the aromatic structure of biochar and CIP molecules may proceed during the adsorption process (Jin et al. 2015; Tran et al. 2017a; Yang et al. 2019). Besides, both biochar owned variety of other functional groups, including C=O, C–O–C, C–N, C=N, C–OH, and C≡N. These functional groups may form an H–bond with moieties (–COOH, –NH–, –F) of CIP molecules, which would contribute to a higher CIP adsorption ability (Yang et al. 2012). More importantly, the ion exchange may happen in the adsorbing process. The piperazine rings of CIP molecules were positively charged (–NH$_2$$^+$–) in neutral or faintly acid solution, and the CIP$^+$ may be attracted by the polar and alkaline surface of biochar with H$^+$ releasing (Fan et al. 2016). Besides, complexation effect of Fe species with CIP molecules may be another removal mechanism. The Fe species probably produce hydrous oxide on the surface of biochar, and one O of the carboxylate group in CIP molecule will bind with the hydrous oxide surface easily. The reason may be that CIP molecule tends to form a six-membered ring with an Fe atom through one O of carboxylate group and keto O (Gu and Karthikeyan 2005). The high content of Fe^{2+} on the SBC surface may enhance the complexation reaction and then result in a higher adsorption.

Heavy metal risk analysis

Literature reported that most of HMs were enriched in the sludge biochar obtained from pyrolysis (Wang et al. 2016). In order to evaluate the potential risks for biochar utilization, HM (Zn, Cr, Ni, As, and Cd) speciation was investigated (Fig. 6), as well as other characteristics including the total concentration (Table S1), leaching toxicity (Table S2), and ecological risks assessment (Table S3) of SL, SLC, and SBC. Figure 6 shows that F4 of all the HMs in SLC and SBC increased significantly after pyrolysis compared with SL. Furthermore, compared with the SLC, the F4 (residual fraction) content of Cr increased dramatically in SBC. A F4 percentage of over 95% of Cr was obtained in SBC, which was 40% higher than that in SLC. For Cd and As, F4 content of STC was much higher than that of SL and reduced further after co-pyrolysis with BW. However, the chemical speciation of Zn and Ni had little distinction by comparison of SLC with SBC, while their F4 speciation increased significantly after pyrolysis. The above result suggested that the HMs, especially
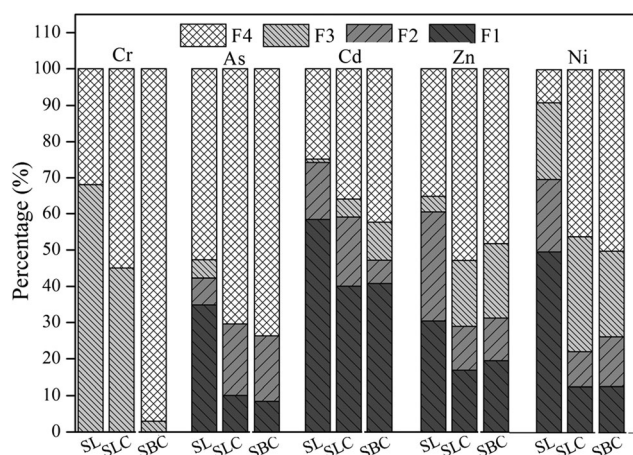

Fig. 6 Distributions of HM speciation in SL, SLC, and SBC (F1, acid-soluble/exchangeable fraction; F2, reducible fraction; F3, oxidizable fraction; F4, residual fraction)

the Cr, Cd, and As, were well immobilized through the co-pyrolysis of SL with BW. As for the leaching toxicity, the leached amount of the HMs in biochar was found to be much lower than that in SL, and the leaching concentrations of HMs in biochar were within the threshold prescribed by GB 5085.3-2007 (Table S1). On the other hand, according to the indices of RI in Table S3, it can be found that the values of RI are in the order of SL > SLC > SBC, and the RI of SBC was close to 50, indicating a low ecological risk in the environment. The above results implied that the SBC possessed a good CIP adsorption ability, and its ecological risk is low when used in the environment.

Conclusions

The biochar obtained from co-pyrolysis of SL and BW was used for ciprofloxacin adsorption. The results confirmed that BW was an outstanding addictive to prepare co-pyrolysis biochar for CIP adsorption and HM immobilization. Ninety-five percent of the CIP was removed from aqueous solutions by SBC with the maximum adsorption capacity of 62.48 mg/g, and the immobilization of Cr, Cd, and As was enhanced in SBC. Moreover, the pseudo-second-order and Freundlich model exhibited better fitting for CIP adsorption onto sludge-based biochar, indicating that this process was involved in chemical and multilayer adsorption. Moreover, the functional groups and Fe species on the biochar surface probably dominated the CIP adsorption; and the π-π interaction, H–bond, ion exchange, and Fe-complexation may happen between the interaction of these functional species and CIP molecules. This work suggests that it is feasible to utilize the sludge-based biochar, especially the co-pyrolyzed SBC, as a potential adsorbent for CIP adsorption from aqueous solutions.

References

Afzal MZ, Sun X, Liu J, Song C, Wang S, Javed A (2018) Enhancement of ciprofloxacin sorption on chitosan/biochar hydrogel beads. Sci Total Environ 639:560–569. https://doi.org/10.1016/j.scitotenv.2018.05.129

Agrafioti E, Kalderis D, Diamadopoulos E (2014) Ca and Fe modified biochars as adsorbents of arsenic and chromium in aqueous solutions. J Environ Manag 146:444–450. https://doi.org/10.1016/j.jenvman.2014.07.029

Ahmad M, Lee SS, Dou X, Mohan D, Sung JK, Yang JE, Ok YS (2012) Effects of pyrolysis temperature on soybean stover- and peanut shell-derived biochar properties and TCE adsorption in water. Bioresour Technol 118:536–544. https://doi.org/10.1016/j.biortech.2012.05.042

Chang KL et al (2014) Rice straw-derived activated carbons for the removal of carbofuran from an aqueous solution. New Carbon Mater 29:47–54. https://doi.org/10.1016/S1872-5805(14)60125-6

Cheung WH, Szeto YS, McKay G (2007) Intraparticle diffusion processes during acid dye adsorption onto chitosan. Bioresour Technol 98:2897–2904. https://doi.org/10.1016/j.biortech.2006.09.045

Dementjev AP, De Graaf A, Van de Sanden MCM, Maslakov KI, Naumkin AV, Serov AA (2000) X-ray photoelectron spectroscopy reference data for identification of the C_3N_4 phase in carbon-nitrogen films. Diam Relat Mater 9:1904–1907. https://doi.org/10.1016/S0925-9635(00)00345-9

Dou X, Chen D, Hu Y, Feng Y, Dai X (2017) Carbonization of heavy metal impregnated sewage sludge oriented towards potential co-disposal. J Hazard Mater 321:132–145. https://doi.org/10.1016/j.jhazmat.2016.09.010

Espinosa K et al (2015) Fluoroquinolone resistance in neisseria gonorrhoeae after cessation of ciprofloxacin usage in San Francisco: using molecular typing to investigate strain turnover. Sex Transmitted Dis 42:57–63. https://doi.org/10.1097/OLQ.0000000000000233

Fan S et al (2016) Biochar prepared from co-pyrolysis of municipal sewage sludge and tea waste for the adsorption of methylene blue from aqueous solutions: kinetics, isotherm, thermodynamic and mechanism. J Mol Liq 220:432–441. https://doi.org/10.1016/j.molliq.2016.04.107

Foo KY, Hameed BH (2010) Insights into the modeling of adsorption isotherm systems. Chem Eng J 156:2–10. https://doi.org/10.1016/j.cej.2009.09.013

Frišták V, Pipíška M, Soja G (2018) Pyrolysis treatment of sewage sludge: a promising way to produce phosphorus fertilizer. J Clean Prod 172:1772–1778. https://doi.org/10.1016/j.jclepro.2017.12.015

Fulazzaky MA (2011) Determining the resistance of mass transfer for adsorption of the surfactants onto granular activated carbons from hydrodynamic column. Chem Eng J 166:832–840. https://doi.org/10.1016/j.cej.2010.11.052

Fulazzaky MA, Khamidun MH, Omar R (2013) Understanding of mass transfer resistance for the adsorption of solute onto porous material from the modified mass transfer factor models. Chem Eng J 228:1023–1029. https://doi.org/10.1016/j.cej.2013.05.100

Fulazzaky MA, Majidnia Z, Idris A (2017) Mass transfer kinetics of Cd (II) ions adsorption by titania polyvinylalcohol-alginate beads from aqueous solution. Chem Eng J 308:700–709. https://doi.org/10.1016/j.cej.2016.09.106

Fytili D, Zabaniotou A (2008) Utilization of sewage sludge in EU application of old and new methods-a review. Renew Sust Energ Rev 12:116–140. https://doi.org/10.1016/j.rser.2006.05.014

Grosvenor AP, Kobe BA, Biesinger MC, McIntyre NS (2004) Investigation of multiplet splitting of Fe 2p XPS spectra and bonding in iron compounds. Surf Interface Anal 36:1564–1574. https://doi.org/10.1002/sia.1984

Gu C, Karthikeyan KG (2005) Sorption of the antimicrobial ciprofloxacin to aluminum and iron hydrous oxides. Environ Sci Technol 39:9166–9173. https://doi.org/10.1021/es051109f

Haghseresht F, Lu GQ (1998) Adsorption characteristics of phenolic compounds onto coal-reject-derived adsorbents. Energy Fuel 12:1100–1107. https://doi.org/10.1021/ef9801165

Hairuddin MN, Mubarak NM, Khalid M, Abdullah EC, Walvekar R, Karri RR (2019) Magnetic palm kernel biochar potential route for

phenol removal from wastewater. Environ Sci and Pollut R 26: 35183–35197. https://doi.org/10.1007/s11356-019-06524-w

Han L, Ro KS, Sun K, Sun H, Wang Z, Libra JA, Xing B (2016) New evidence for high sorption capacity of hydrochar for hydrophobic organic pollutants. Environ Sci Technol 50:13274–13282. https://doi.org/10.1021/acs.est.6b02401

He S, Zhang D, Gu L, Zhang S, Yu X (2012) Bromate adsorption using Fe-pillared bentonite. Environ Technol 33:2337–2344. https://doi.org/10.1080/09593330.2012.666571

Huang HJ, Yang T, Lai FY, Wu GQ (2017) Co-pyrolysis of sewage sludge and sawdust/rice straw for the production of biochar. J Anal Appl Pyrolysis 125:61–68. https://doi.org/10.1016/j.jaap.2017.04.018

Jiang J, Zhang L, Wang X, Holm N, Rajagopalan K, Chen F, Ma S (2013) Highly ordered macroporous woody biochar with ultra-high carbon content as supercapacitor electrodes. Electrochim Acta 113:481–489. https://doi.org/10.1016/j.electacta.2013.09.121

Jin Z, Wang X, Sun Y, Ai Y, Wang X (2015) Adsorption of 4-n-nonylphenol and bisphenol-A on magnetic reduced graphene oxides: a combined experimental and theoretical studies. Environ Sci Technol 49:9168–9175. https://doi.org/10.1021/acs.est.5b02022

Jin J, Wang M, Cao Y, Wu S, Liang P, Li Y, Zhang J, Zhang J, Wong MH, Shan S, Christie P (2017) Cumulative effects of bamboo sawdust addition on pyrolysis of sewage sludge: biochar properties and environmental risk from metals. Bioresour Technol 228:218–226. https://doi.org/10.1016/j.biortech.2016.12.103

Karri RR, Sahu JN, Jayakumar NS (2017) Optimal isotherm parameters for phenol adsorption from aqueous solutions onto coconut shell based activated carbon: error analysis of linear and non-linear methods. J Taiwan Inst Cheme 80:472–487. https://doi.org/10.1016/j.jtice.2017.08.004

Li M, Wei D, Du Y (2014) Acute toxicity evaluation for quinolone antibiotics and their chlorination disinfection processes. J Environ Sci (China) 26:1837–1842. https://doi.org/10.1016/j.jes.2014.06.023

Li T, Han X, Liang C, Shohag MJI, Yang X (2015a) Sorption of sulphamethoxazole by the biochars derived from rice straw and alligator flag. Environ Technol 36:245–253. https://doi.org/10.1080/09593330.2014.943299

Li X, Chen S, Fan X, Quan X, Tan F, Zhang Y, Gao J (2015b) Adsorption of ciprofloxacin, bisphenol and 2-chlorophenol on electrospun carbon nanofibers: in comparison with powder activated carbon. J Colloid Interface Sci 447:120–127. https://doi.org/10.1016/j.jcis.2015.01.042

Li C, Wang X, Zhang G, Yu G, Lin J, Wang Y (2017a) Hydrothermal and alkaline hydrothermal pretreatments plus anaerobic digestion of sewage sludge for dewatering and biogas production: bench-scale research and pilot-scale verification. Water Res 117:49–57. https://doi.org/10.1016/j.watres.2017.03.047

Li R, Wang Z, Guo J, Li Y, Zhang H, Zhu J, Xie X (2017b) Enhanced adsorption of ciprofloxacin by KOH modified biochar derived from potato stems and leaves. Water Sci Technol 77:1127–1136. https://doi.org/10.2166/wst.2017.636

Li J, Yu G, Pan L, Li C, You F, Xie S, Wang Y, Ma J, Shang X (2018) Study of ciprofloxacin removal by biochar obtained from used tea leaves. J Environ Sci (China) 73:20–30. https://doi.org/10.1016/j.jes.2017.12.024

Li J, Pan L, Yu G, Xie S, Li C, Lai D, Li Z, You F, Wang Y (2019) The synthesis of heterogeneous Fenton-like catalyst using sewage sludge biochar and its application for ciprofloxacin degradation. Sci Total Environ 654:1284–1292. https://doi.org/10.1016/j.scitotenv.2018.11.013

Liao X, Li B, Zou R, Dai Y, Xie S, Yuan B (2016) Biodegradation of antibiotic ciprofloxacin: pathways, influential factors, and bacterial community structure. Environ Sci and Pollut R 23:7911–7918. https://doi.org/10.1007/s11356-016-6054-1

Luo K et al (2019) Enhanced ciprofloxacin removal by sludge-derived biochar: effect of humic acid. Chemosphere 231:495–501. https://doi.org/10.1016/j.chemosphere.2019.05.151

Mao H, Wang S, Lin JY, Wang Z, Ren J (2016) Modification of a magnetic carbon composite for ciprofloxacin adsorption. J Environ Sci (China) 49:179–188. https://doi.org/10.1016/j.jes.2016.05.048

Miskolczi N, Nagy R (2012) Hydrocarbons obtained by waste plastic pyrolysis: comparative analysis of decomposition described by different kinetic models. Fuel Process Technol 104:96–104. https://doi.org/10.1016/j.fuproc.2012.04.031

Nasuha N, Hameed BH, Din ATM (2010) Rejected tea as a potential low-cost adsorbent for the removal of methylene blue. J Hazard Mater 175:126–132. https://doi.org/10.1016/j.jhazmat.2009.09.138

Ngeno EC, Orata F, Baraza LD, Shikuku VO, Jemutai S (2016) Adsorption of caffeine and ciprofloxacin onto pyrolitically derived water hyacinth biochar: isothermal, kinetic and thermodynamic studies. J Chem 10:185–194. https://doi.org/10.17265/1934-7375/2016.04.006

Pan LJ, Li J, Li CX, Tang XD, Yu GW, Wang Y (2018) Study of ciprofloxacin biodegradation by a Thermus sp. isolated from pharmaceutical sludge. J Hazard Mater 343:59–67. https://doi.org/10.1016/j.jhazmat.2017.09.009

Ren N, Tang Y, Li M (2018) Mineral additive enhanced carbon retention and stabilization in sewage sludge-derived biochar. Process Saf Environ Prot 115:70–78. https://doi.org/10.1016/j.psep.2017.11.006

Shang JG, Kong XR, He LL, Li WH, Liao QJH (2016) Low-cost biochar derived from herbal residue: characterization and application for ciprofloxacin adsorption. Int J Environ Sci Te 13:2449–2458. https://doi.org/10.1007/s13762-016-1075-3

Shen B, Tian L, Li F, Zhang X, Xu H, Singh S (2017) Elemental mercury removal by the modified bio-char from waste tea. Fuel 187:189–196. https://doi.org/10.1016/j.fuel.2016.09.059

Srivastava VC, Swamy MM, Mall ID, Prasad B, Mishra IM (2006) Adsorptive removal of phenol by bagasse fly ash and activated carbon: equilibrium, kinetics and thermodynamics. Colloids Surf Physicochem Eng Aspects 272:89–104. https://doi.org/10.1016/j.colsurfa.2005.07.016

Sun Y, Li H, Li G, Gao B, Yue Q, Li X (2016) Characterization and ciprofloxacin adsorption properties of activated carbons prepared from biomass wastes by H_3PO_4 activation. Bioresour Technol 217: 239–244. https://doi.org/10.1016/j.biortech.2016.03.047

Thines KR, Abdullah EC, Mubarak NM, Ruthiraan M (2017) Synthesis of magnetic biochar from agricultural waste biomass to enhancing route for waste water and polymer application: a review. Renew Sust Energ Rev 67:257–276. https://doi.org/10.1016/j.rser.2016.09.057

Thommes M, Kaneko K, Neimark AV, Olivier JP, Rodriguez-Reinoso F, Rouquerol J, Sing KSW (2015) Physisorption of gases, with special reference to the evaluation of surface area and pore size distribution (IUPAC Technical Report). Pure Appl Chem 87:1051–1069. https://doi.org/10.1515/pac-2014-1117

Tran HN, Wang YF, You SJ, Chao HP (2017a) Insights into the mechanism of cationic dye adsorption on activated charcoal: the importance of π-π interactions. Process Saf Environ Prot 107:168–180. https://doi.org/10.1016/j.psep.2017.02.010

Tran HN, You S, Hosseini-Bandegharaei A, Chao H (2017b) Mistakes and inconsistencies regarding adsorption of contaminants from aqueous solutions: a critical review. Water Res 120:88–116. https://doi.org/10.1016/j.watres.2017.04.014

Tu J, Yang Z, Hu C, Qu J (2014) Characterization and reactivity of biogenic manganese oxides for ciprofloxacin oxidation. J Environ Sci (China) 26:1154–1161. https://doi.org/10.1016/S1001-0742(13)60505-7

Wang X, Li C, Zhang B, Lin J, Chi Q, Wang Y (2016) Migration and risk assessment of heavy metals in sewage sludge during hydrothermal treatment combined with pyrolysis. Bioresour Technol 221:560–567. https://doi.org/10.1016/j.biortech.2016.09.069

Wang G, Yu G, Xie S, Jiang R, Wang Y (2019a) Effect of co-pyrolysis of different plastics with sewage sludge on heavy metals in the biochar. J Fuel Chem Technol 47:611–620. http://manu60.magtech.com.cn/rlhxxb/EN/abstract/abstract29395.shtml#. Accessed 10 Dec 2018

Wang X, Chi Q, Liu X, Wang Y (2019b) Influence of pyrolysis temperature on characteristics and environmental risk of heavy metals in pyrolyzed biochar made from hydrothermally treated sewage sludge. Chemosphere 216:698–706. https://doi.org/10.1016/j.chemosphere.2018.10.189

Wang X, Li C, Li Z, Yu G, Wang Y (2019c) Effect of pyrolysis temperature on characteristics, chemical speciation and risk evaluation of heavy metals in biochar derived from textile dyeing sludge. Ecotoxicol Environ Saf 168:45–52. https://doi.org/10.1016/j.ecoenv.2018.10.022

Xie S, Yu G, Li C, You F, Li J, Tian R, Wang G, Wang Y (2019) Dewaterability enhancement and heavy metals immobilization by pig manure biochar addition during hydrothermal treatment of sewage sludge. Environ Sci and Pollut R 26:16537–16547. https://doi.org/10.1007/s11356-019-04961-1

Yamashita T, Hayes P (2008) Analysis of XPS spectra of Fe^{2+} and Fe^{3+} ions in oxide materials. Appl Surf Sci 254:2441–2449. https://doi.org/10.1016/j.apsusc.2007.09.063

Yang W, Lu Y, Zheng F, Xue X, Li N, Liu D (2012) Adsorption behavior and mechanisms of norfloxacin onto porous resins and carbon nanotube. Chem Eng J 179:112–118. https://doi.org/10.1016/j.cej.2011.10.068

Yang Z, Xing R, Zhou W (2019) Adsorption of ciprofloxacin and Cu^{2+} onto biochars in the presence of dissolved organic matter derived from animal manure. Environ Sci and Pollut R 26:14382–14392. https://doi.org/10.1007/s11356-019-04760-8

You FT, Yu GW, Wang Y, Xing ZJ, Liu XJ, Li J (2017) Study of nitric oxide catalytic oxidation on manganese oxides-loaded activated carbon at low temperature. Appl Surf Sci 413:387–397. https://doi.org/10.1016/j.apsusc.2017.04.044

Zeng Z et al (2018) Comprehensive adsorption studies of doxycycline and ciprofloxacin antibiotics by biochars prepared at different temperatures. Front Chem 6:1–11. https://doi.org/10.3389/fchem.2018.00080

Zhang B, Han X, Gu P, Fang S, Bai J (2017) Response surface methodology approach for optimization of ciprofloxacin adsorption using activated carbon derived from the residue of desilicated rice husk. J Mol Liq 238:316–325. https://doi.org/10.1016/j.molliq.2017.04.022

Zhao B, Xu X, Zeng F, Li H, Chen X (2018) The hierarchical porous structure bio-char assessments produced by co-pyrolysis of municipal sewage sludge and hazelnut shell and Cu (II) adsorption kinetics. Environ Sci and Pollut R 25:19423–19435. https://doi.org/10.1007/s11356-018-2079-y

Zhu X, Tsang DCW, Chen F, Li S, Yang X (2015) Ciprofloxacin adsorption on graphene and granular activated carbon: kinetics, isotherms, and effects of solution chemistry. Environ Technol 36:3094–3102. https://doi.org/10.1080/09593330.2015.1054316